PCCP

Accepted Manuscript

ROYAL SOCIETY OF CHEMISTRY

www.rsc.org/pccp

Relative stability and reducibility of CeO_2 and Rh/CeO_2 species on the surface and in the cavities of γ-Al_2O_3: A periodic DFT study

Iskra Z. Koleva,[a] Hristiyan A. Aleksandrov,[a] Georgi N. Vayssilov, [a,*] Renata Duarte,[b] Jeroen A. van Bokhoven[b,c,*]

[a] Faculty of Chemistry and Pharmacy, University of Sofia, 1126 Sofia, Bulgaria
e-mail: gnv@chem.uni-sofia.bg

[b] Institute for Chemical and Bioengineering, ETH Zurich, Zurich, Switzerland

[c] Laboratory for Catalysis and Sustainable Chemistry, Swiss Light Source, Paul Scherrer Institute, Villigen, Switzerland, j.a.vanbokhoven@chem.ethz.ch

Abstract

We report the structure and stability of ceria units deposited on the surface of γ-Al_2O_3 respectively incorporated in its cavities, as determined by periodic density functional calculations. Ceria species are modeled as CeO_2 or Ce_2O_4 moieties or as a small nanoparticle, $Ce_{13}O_{26}$, on the (100) and (001) surfaces of a γ-Al_2O_3 slab. Among the studied structures the incorporation of Ce^{4+} ions in cavities of γ-Al_2O_3 is favored with respect to the ions on the surface only in subsurface cavities of the (100) surface. The calculations also suggested that formation of a surface layer of ceria on (100) alumina surface is preferable compared to three-dimensional moieties. The deposition of a small ceria nanoparticle on (100) and (001) surfaces of γ-Al_2O_3 reduces the energy for oxygen vacancy formation to an essentially spontaneous process on the (100) surface, which may be the reason for the experimentally detected large fraction of Ce^{3+} ions in the CeO_2/γ-Al_2O_3 systems. The deposition of a single rhodium atom or RhO unit in some of the structures with a CeO_2 unit and $Ce_{13}O_{26}$ showed that spontaneous electron transfer from rhodium to cerium ion occurs, which results in reduction of Ce^{4+} to Ce^{3+} and the oxidation of rhodium. Only in the presence of deposited rhodium atoms, the incorporated cerium ions may be reduced to Ce^{3+}.

1. Introduction

The high catalytic performance of ceria based materials in various processes is due to the ability of cerium cation to change reversibly its oxidation state between +4 and +3, which allows the material to release and store oxygen.[1] This property of ceria is widely used in three-way catalysts (TWCs),[2,3] water-gas shift reaction, solid oxide fuel cells,[4,5] etc. TWCs significantly decrease the air pollution from automobile exhaust by oxidizing hydrocarbons and carbon monoxide and reducing nitrogen oxides, and thus turning them into harmless gases (CO_2, H_2O and N_2). Besides as catalyst, ceria (CeO_2) prevents alumina from sintering and stabilizes supported nano-sized precious metals such as rhodium, palladium and platinum, which are very important for the enhancement of TWCs activity.[6-8]

Alumina is a basic component of TWCs and it is widely used in heterogeneous catalysis[9,10] as a support in the refining and petrochemical industries.[11] In particular, γ-Al_2O_3 is often used as a support of ceria and noble metals since compared to the other aluminum oxides it features higher catalytic activity due to its structural characteristics and its acid-base properties.[12,13,14] CeO_2/γ-Al_2O_3 catalysts are also efficient for the dehydrogenation of ethane to ethylene.[15] Rh/γ-Al_2O_3–CeO_2 system had been also investigated as catalyst for the methane steam reforming[16] and the oxidation of methyl tert-butyl ether.[17] Shi et al. modeled deposition of rhodium atom and small clusters on different γ-Al_2O_3 surfaces and shown that the interaction energy and the charge of the metal species depends on the presence of hydroxyls on the surface.[18]

For Rh/CeO_2/Al_2O_3 catalytic system Duarte et al.[16] recently reported that, when a reduced sample containing a significant fraction of Ce^{3+} ions is exposed to oxygen only part of the Ce^{3+} species are converted to Ce^{4+}, while a substantial amount of cerium ions remains in oxidation state +3. This finding was rationalized with the fact that most probably part of ceria species is embedded into the alumina matrix. Such incorporation may stabilize the alumina against sintering at high temperature. Hence the cooling to room temperature in the presence of oxygen causes re-oxidation only of the Ce^{3+} ions located in ceria species on the alumina surface, while the Ce^{3+} cations incorporated in the γ-alumina remain reduced.[16] Moreover, under reaction conditions, a significant fraction of cerium was reduced. Only a very small fraction, about 2% of the total cerium, re-oxidized after switching the feed to a stream containing water, which indicates that only a small fraction of ceria participates in the activation of water. To shed light on these phenomena, we studied the structure and stability

of ceria units deposited on the surface of γ-Al_2O_3 or incorporated in its cavities using periodic density functional calculations. Ceria species are modeled as CeO_2 or Ce_2O_4 moieties or a small nanoparticle, $Ce_{13}O_{26}$, on (100) and (001) surfaces of γ-Al_2O_3. This allows us to check whether the process of incorporation of ceria units in the internal cavities of γ-Al_2O_3 is favorable. Reduction of ceria species after removal of oxygen and exchange of cerium ions by aluminum ions is also considered. The influence of cerium and rhodium oxidation state is also determined after deposition of a single rhodium atom or of a RhO moiety in some of the structures with a CeO_2 unit and $Ce_{13}O_{26}$ nanoparticle.

2. Model and computational method

In the periodic DFT calculations we employed a crystal structure of bulk γ-Al_2O_3 with space group P21/m and the following unit cell parameters: a = 5.587 Å, b = 8.413 Å, c = 8.068 Å, β = 90.59◦, according to Digne et al.[19] In our model we use double unit cell size in all directions. The slab models for (100) and (001) surfaces of γ-Al_2O_3 are cut perpendicular to direction a and c, respectively. The parameters of the optimized two simulation cells are 11.046 * 16.650 * 16.016 $Å^3$ in size and contain additional 10 Å vacuum space in directions a and c between the slabs for (100) and (001) models, respectively. Both slab models contain 64 Al_2O_3 units (320 atoms). With this size the supercells are by about 50 % bigger than those employed by Shi et al. for modeling of rhodium clusters on alumina.[18] Periodic DFT+U calculations were performed with the generalized gradient-corrected exchange-correlation functional Perdew-Wang 91 (PW91),[20,21] as implemented in the Vienna Ab Initio Simulation Package (VASP).[22-25] The U parameter was set to 4.0 eV, as in previous model studies of ceria systems.[26,27] The valence wave functions were expanded to a plane wave basis with energy cut-off of 415 eV. Pseudopotentials within the projector augmented waves (PAW) approach are employed for the description of electron–ion interactions.[28] The Brillouin zone was sampled to (1×1×1) Monkhorst-Pack grid.[29] Where appropriate, e.g. structures containing reduced ceria species and/or rhodium atom, spin-polarized calculations are performed. We performed benchmark calculations with 1×3×3 k-mesh for the optimized structures A-13a and A-13c (see below for notation of the structures) and the calculated energy difference between the two structures agrees within 0.002 eV with that calculated with 1×1×1 k-mesh. In order to check the influence of the energy cut-off on the results we also calculated the energies of the same structures with energy cut-off of 600 eV and the energy difference between the two structures agrees within 0.003 eV with that calculated with cut-off of 415 eV.

The relative energies for incorporation of CeO_2 unit(s) or exchange of cerium ion with Al^{3+} ion is calculated by the following expression:

$\Delta E = E_{cav} - E_{dep}$,

where E_{cav} is the energy of the structure with incorporated ceria unit(s) in the cavities or with exchange of cerium ion with Al^{3+} ion and E_{dep} is the energy of the structure with the corresponding species deposited on the surface.

The stability of the reduced species is estimated by the energy for formation of a single oxygen vacancy:

$$E_{vac} = E_{Ce_xO_{2x-1}} + \frac{1}{2}E_{O_2} - E_{Ce_xO_{2x}}$$

where $E_{Ce_xO_{2x-1}}$ and $E_{Ce_xO_{2x}}$ are the total energies of the reduced and stoichiometric structure with deposited units/nanoparticle, respectively, and E_{O_2} is the total energy of an isolated oxygen molecule.

The adsorption energy of a rhodium atom on CeO_2/Al_2O_3 system, E_{ads}, is calculated with respect to the corresponding initial CeO_2/Al_2O_3 structure and an isolated rhodium atom. For all energy characteristics a negative value corresponds to an exothermic process.

The average displacement of Al and O ions of γ-Al_2O_3 is calculated in following way:

$$\langle r \rangle = \frac{\sum\sqrt{\Delta x^2+\Delta y^2+\Delta z^2}}{n},$$

where $\Delta x/y/z$ is the difference in the position of one Al or O ion along x/y/z axes between the structure with deposited or incorporated ceria species and in the optimized pristine γ-Al_2O_3, and n is the number of ions included in the analysis of the displacement.

For the different structures we use the following notation: a capital letter denoting the type of the modeled alumina surface - A for (100) and B for (001), a number denoting the number of cerium ions in the model (1, 2, 4 or 13) followed by a small letter showing consecutive number of the structure with the corresponding composition. For example the structure B-13a is the first model that contains 13 cerium cations in the ceria nanoparticle on γ-Al_2O_3(001) surface.

3. Results

Figure 1a,b shows the top and side views of the clean (100) and (001) surfaces of γ-Al_2O_3. In the (100) surface the exposed aluminum cations have coordination numbers 3, 4 or 5, while on (001) surface only five- and four-coordinated aluminum ions are exposed. All optimized structures are shown in the ESI, Figs. S1 to S5, and some selected structures are shown in Figs. 2 to 6. In this section, we first present the results for deposited stoichiometric monomer CeO_2 and dimer Ce_2O_4 species (Table 1) and ceria nanoparticle (Table 2) on γ-Al_2O_3(100) surface. Next, we consider analogues structures on the (001) surface (Tables 3 and 4). The last part of this section is devoted to several models of deposited rhodium on the CeO_2/Al_2O_3 (Table 5).

3.1. Ceria species on the γ-Al_2O_3(100) surface

3.1.1. Stoichiometric CeO_2 and Ce_2O_4 units

The deposition of a single CeO_2 unit on the γ-Al_2O_3(100) surface (Fig. 2, str. A-1a) resulted in coordination of the cerium ion to one additional oxygen ion from the alumina surface, while each of the oxygen ions from the ceria unit is bound to cerium and one surface aluminum cation. When the CeO_2 unit is incorporated in a subsurface cavity the local structure of the alumina framework around it changes considerably during the geometry optimization and the Ce^{4+} cation approaches the surface (Fig. 2, str. A-1b). The obtained structure A-1b is by 1.3 eV more stable than the structure A-1a with CeO_2 unit deposited on the surface (Table 1). The incorporation of CeO_2 in an internal cavity of the γ-Al_2O_3 (Fig. 2, str. A-1c) is, however, disfavored by 2.4 eV compared to the structure A-1a, likely due to stronger distortion of the surrounding of the cerium ion inside the alumina. As a quantitative measure of distortion of the alumina slab upon interaction with ceria species we used the average displacement of aluminum and oxygen ions. The average displacements of the aluminum and oxygen (the values for oxygen ions are shown in parentheses after the values for aluminum ions) ions for the structures with one unit in a subsurface, A-1b and one unit in an internal cavity, A-1c, are larger respectively by 8.1 (5.6) pm and 14.4 (13.0) pm compared to the displacement in the structure with deposited unit (see Table S1). Thus, the higher stability of the cerium ion in the subsurface cavity, A-1b, may be explained by two factors: the larger number of Ce-O contacts, eight, compared to three for the structure with the cerium ion on the surface, and minor distortion of the alumina framework, compared the structure with cerium ion in an internal cavity, A-1c.

We also studied an exchange of Ce^{4+} cation from the CeO_2 deposited unit with different Al^{3+} cations from γ-Al_2O_3 (Fig. S1, str. A-1d to A-1i, and Fig. 2, str. A-1d). An exchange of Al^{3+} ions from the surface, which are coordinated to only three oxygen centers (Fig. 2, str. A-1d), is exothermic by -0.7 eV compared to the structure A-1a with CeO_2 unit on (100) surface. The structures A-1e and A-1f, in which cerium ion is exchanged with surface Al^{3+} cations coordinated to five oxygen centers are close in energy to the structure with the deposited CeO_2 unit (Table 1). An exchange of Ce^{4+} with aluminum cations inside the alumina slab is an unfavorable process by 1.1-2.8 and 4.7 eV when the corresponding aluminum ion is 4- and 6-coordinated, respectively (Table 1, Fig. S1, str. A-1g to A-1i).

In the modeled structures with two CeO_2 units on the γ-Al_2O_3(100) surface the two cerium ions are connected by an oxygen atom (Fig. 2, str. A-2a). The incorporation of one or both CeO_2 units into the subsurface region respectively in the bulk of the alumina slab is endothermic with respect to structure A-2a. The structure A-2b (Fig. S2), in which one of the two CeO_2 units is incorporated in the subsurface cavity, is by 1.6 eV less stable than A-2a. To minimize eventual repulsion between ceria units in the structure A-2d we incorporated one CeO_2 unit in a subsurface and the other one in an internal cavity in such a way that they are located along the diagonal of the slab with Ce-Ce distance longer than 1000 pm (Fig. S2, str. A-2d). In this case we also moved one of the oxygen centers from each CeO_2 unit in a different cavity, in order to reduce the repulsion inside the cavities. Again, the structure is less stable by 2.9 eV compared to the structure A-2a. The incorporation of both ceria units in internal cavities in the structure A-2e (Fig. S2) is even more endothermic process, ΔE = 4.5 eV.

In all structures the presence of ceria in the cavities of alumina causes notable deformation of the (100) surface, which is the likely reason for the endothermicity of the process. As in the case with one ceria unit, the displacements of the aluminum and oxygen ions are larger for the structures with two species in cavities compared to the deposited ceria species. Thus, the displacement of Al (O) ions in the structures with ceria units in subsurface (A-2c) and in internal cavities (A-1e) is 20.4 (19.7) pm and 25.5 (26.8) pm, respectively.

3.1.2. Reduced ceria species

The models of the reduced ceria species were constructed by removing an oxygen atom from the structures with two CeO_2 units, which resulted in an oxidation state of +3 for both cerium

ions (Fig. S2, str. A-2f to A-2i). The energy for removal of one of the oxygen atoms from the structure of deposited Ce_2O_4 unit on the alumina surface resulting in the structure A-2f (Fig. 2), E_{vac} = 3.1 eV (Table 1), is significantly higher than the energy for oxygen removal from slabs representing a CeO_2(111) surface, 2.6 eV,[27,30,31] a CeO_2(100) surface, 2.7 eV,[29] and a CeO_2(110) surface, 1.99 eV.[30] The structure with one Ce^{3+} in subsurface cavity, A-2g, has E_{vac} = 3.6 eV (with respect to A-2a) and is by 0.5 eV less stable than structure with deposited reduced ceria species, A-2f. The structure where both Ce^{3+} cations are located in cavities of alumina or both cerium cations exchanged with aluminum (Figs. S2, A-2h and A-2i) are notably less stable compared to the structure with Ce^{3+} cations on the surface, by 5.8 and 5.2 eV, respectively. Consequently, the E_{vac} values for the latter structures are higher than 8.0 eV with respect to the most stable stoichiometric structure A-2a (Table 1). Thus, the reduction of the small Ce_2O_4 unit either on the surface of alumina or in subsurface cavities is energetically unfavorable compared to extended ceria surfaces.

3.1.3. Stoichiometric ceria nanoparticle

As a model of larger ceria structures we used a small ceria nanoparticle, $Ce_{13}O_{26}$. Taking into account the size of Al_2O_3(100) surface within our simulation cell, our model corresponds to a coverage of about 30% of alumina surface by ceria. The initial structure of this nanoparticle was taken from the top two ceria layers of the larger nanoparticles, used in earlier calculations.[26,32] The top layer is formed by four cerium ions and the bottom layer, which is in contact with Al_2O_3(100) surface, has nine cerium ions (See Fig. 3, str. A-13a). We also modeled two structures with one CeO_2 unit moved from the top of the ceria nanoparticle (from structure A-13a) to different positions of the alumina surface. Both structures, denoted as A-13a' and A-13a", were found more stable than the initial structure with intact deposited ceria nanoparticle by 0.9 and 1.8 eV, respectively. This may suggest that ceria species deposited on Al_2O_3(100) prefer bonding to the surface instead of growing three-dimensional.

Starting from deposited ceria nanoparticle (structure A-13a), the incorporation of one or two units in subsurface cavities, taken from the top layer of the ceria nanoparticle is a favorable process (Table 2) with energy gain of 1.4 eV (Fig. 3, str. A-13b) and 0.6 eV (Fig. 3, str. A-13c), respectively. However, those structures are less stable than the model A-13a". Since the ions from the ceria nanoparticle interact with large a part of the surface centers of the alumina, the mobility of the latter centers is restricted and their positions are not changed significantly upon incorporation of the CeO_2 unit in subsurface cavity. Indeed, the average

displacement of the Al and O ions either on the surface or all ions in the slab upon incorporation of ceria units is smaller compared to the structures with one and two ceria units, described in the previous section. The difference in the deviations of the Al (O) centers between the structures with deposited nanoparticle and one unit in a subsurface cavity (str. A-1b) and the corresponding structure with one CeO_2 unit (A-1b) is small, 8.6 (8.4) pm (see Table S1). The deviations of the positions of all Al (O) ions in the structure with deposited nanoparticle and two units in the internal cavities of alumina (str. A-13c) is by 12.4 (14.0) pm, smaller compared to the corresponding values for the structure with two CeO_2 units in subsurface cavities (str. A-2b) and by 17.5 (21.2) pm compared to the structure with two CeO_2 units in internal cavities (str. A-2c).

The exchange of different Ce^{4+} cations from the deposited $Ce_{13}O_{26}$ nanoparticle with Al^{3+} cation from the bulk, which is bound to four oxygen ions, is also modeled (Fig. 3, str. A-13d and Fig. S3, str. A-13e to A-13i). In general, the process of Ce^{4+} exchange with Al^{3+} is energy neutral or slightly endothermic, by 0.0-0.4 eV, for the structures with exchanged Ce^{4+} from the top of the nanoparticle, as in structures A-13d to A-13g (Table 2). The endothermicity of this process is notably higher for the structures with exchanged Ce^{4+} from the bottom of the ceria nanoparticle, structures A-13h and A13i; here the ΔE values are 1.5 and 1.9 eV, respectively.

3.1.4. Reduced ceria nanoparticles

To mimic oxygen release from the ceria nanoparticle, as in the case with two ceria units, we removed one oxygen anion creating two Ce^{3+} cations. In structures A-13j (Fig. 3) and A-13k (Fig. S3, A-13k) the oxygen atoms were removed from the positions found the most preferable for the bare $Ce_{21}O_{42}$ nanoparticle, which are the low-coordinated oxygen atoms interacting with two cerium ions.[27,31,33] The removed oxygen atoms are from the top of the nanoparticle and in both structures one of the Ce^{3+} cations is on the top of the nanoparticle, while the other one is located in the bottom layer. These two structures are very close in energy, within 0.1 eV (Table 2).

The structure A-13l (Fig. S3) is obtained from structure A-13k by incorporating one CeO_2 unit in a subsurface cavity of the alumina support, and has essentially the same stability as the structures A-13j and A-13k. However, the incorporated cerium ion is in oxidation state +4, while similarly to structures A-13j and A-13k, one of the Ce^{3+} ions is on the top of the

ceria nanoparticle and the other one is from the bottom layer. Another structure with reduced ceria (Fig. S3, str. A-13m), is obtained from the stoichiometric structure A-13c (with two CeO_2 units in subsurface cavities) by removing an oxygen atom from the incorporated ceria units. The obtained structure is by 1.0 eV less stable than the most stable reduced model A-13j. One of Ce^{3+} cations in this structure, A-13m, is on the top of the nanoparticle, while the other one is in the cavity. The last modeled structure A-13n (Fig. S3) is obtained from the structure A-13k by exchanging one of the top Ce^{4+} cations with Al^{3+} cation, in the way analogous to the exchange in the stoichiometric structure A-13f. Both Ce^{3+} cations are in the bottom of the nanoparticle and that structure, A-13n, is less stable by 2.7 eV compared to the initial one, A-13k.

The energies for the oxygen vacancy formation, E_{vac}, for the structures A-13j, A-13k and A-13l are low, ~0.2 eV (see Table 2), which suggests that the reduction of the ceria cluster (desorption of oxygen) occurs essentially spontaneously and Ce^{3+} ions are likely to exist in the system. For the structures with one Ce^{3+} in a cavity and with exchanged Ce^{3+} cation, E_{vac} are higher, 1.1 and 3.0 eV, respectively.

Using calculated values we derived enthalpy and entropy (for details see ESI) for the reduced and stoichiometric supported ceria nanoparticles and simulated relative concentration of those species at 300 K (Fig. 7). The results suggest that the concentration of the reduced species under air at atmospheric pressure is 58 % versus 40 % for the stoichiometric nanoparticle. When the temperature is higher than 500 K all ceria nanoparticles are reduced.

According to the analysis of the factors influencing the oxygen vacancy formation in ceria nanoparticles, reported in Ref. 26, there is a correlation of the E_{vac} with the difference between electrostatic field, V, calculated at the oxygen anion with the least negative V(O) value, and the Ce^{4+} cation with most negative V(Ce) value. Namely, E_{vac} decreases with increase of the electrostatic field difference ΔV. By this reason we calculated the electrostatic field at the ceria and oxygen centers in ceria nanoparticle when it is supported on γ-alumina surface and when it is isolated (unsupported). For deposited nanoparticle the ΔV is 14.1 eV, while for isolated ceria nanoparticle ΔV = 13.5 eV. According to the trends, reported earlier,[26] the increase of the ΔV for the nanoparticle upon deposition of γ-alumina surface by 0.6 eV cause decrease of the E_{vac} by 0.8 to 1.7 eV.

3.2. Ceria species on γ-Al_2O_3(001) surface

3.2.1. Stoichiometric CeO_2 and Ce_2O_4 units

Figure 4 shows the structure of the CeO_2 unit on (001) surface, str. B-1a. The cerium ion is coordinated to four oxygen centers including two oxygen centers from alumina surface. Unlike the results for alumina (100) surface, the incorporation of a CeO_2 unit in a subsurface cavity is strongly disfavored process, by 3.8 eV (Table 3), although during the optimization the cerium ion is pushed to the surface (Fig. S4, str. B-1b). The incorporation of a CeO_2 unit in an internal cavity is even more unfavorable by 11.3 eV (Fig. S4, str. B-1c) with respect to CeO_2 unit on the surface.

The incorporation of two ceria units in two identical subsurface cavities is also notably disfavored. The energy difference between the structures with deposited ceria units on the surface and with two incorporated units in cavities (Fig. S4, str. B-2a and B-2b) is 8.1 eV. This is more than twice higher than the value for the incorporation of one unit, 3.8 eV.

We also modeled structures with larger number (four) of ceria units to check whether the incorporation of ceria unit will be facilitated with the increasing the ceria cluster size on the surface (Fig. S4, str. B-4a). Interestingly, the incorporation of one of the CeO_2 units in a subsurface cavity (Fig. 4, str. B-4b) for this structure is notably less endothermic, only 0.7 eV, while for the models with only one or two ceria units the energy difference was 8.1-11.3 eV (Table 3). To some extent this difference may be explained by the small average displacement of Al (O) ions of γ-Al_2O_3 in the structure B-4b with respect to the deposited ceria moiety (B-4a), 6.3 (10.1) pm. For comparison, the corresponding values for structures with one or two units in subsurface cavity, B-1c and B-2b, are 11.6 (11.1) pm and 17.2 (17.2) pm, respectively (Table S1).

3.2.2. Reduced ceria species

The energy for removal of an oxygen atom from the structure with a deposited CeO_2 unit (Fig. 4, str. B-2c) is 2.6 eV, which is by 0.5 eV lower compared to the analogous value for the (100) surface, and is the same as the value calculated for CeO_2(111) slab, 2.6 eV.[31] We also modeled a structure with two Ce^{3+} cations incorporated in two identical cavities (Table 3, Fig. S3, str. B-2d). During the geometry optimization Ce^{3+} cations emerged on the surface, which

is strongly deformed. This structure is less stable by 1.1 eV compared to the structure with two Ce^{3+} cations deposited on the surface (Fig.4, str. B-2c).

3.2.3. Stoichiometric ceria nanoparticle

Figure 5 shows the optimized model of deposited $Ce_{13}O_{26}$ nanoparticle on (001) surface (str. B-13a). Since the exposed Al_2O_3(001) surface in our simulation cell is smaller the exposed (100) surface, the ceria coverage of the models on (001) surface is even higher than that on (100) surface, approaching half of alumina surface covered by ceria. In $Ce_{13}O_{26}/Al_2O_3$(001) models the structure is similar to a ceria nanowire since in one direction the cerium and oxygen ions on the boundary of the cell are connected with the ions from the neighboring unit cell. Besides, there are no well-defined layers of cerium cations. A notable difference with the results for the nanoparticle on γ-Al_2O_3(100) surface is that the incorporation of CeO_2 unit from the ceria nanoparticle in a subsurface cavity is disfavored by 8.7 eV (Table 4, str. B-13b) compared to the $Ce_{13}O_{26}$ nanoparticle deposited on the surface (str. B-13a). The average displacement of the Al (O) ions in the structure B-13b is by 12.2 (10.1) pm larger than the corresponding values for the structure B-13a (Table S1).

The exchange of Ce^{4+} cations from the deposited $Ce_{13}O_{26}$ nanoparticle and an Al^{3+} cation from the bulk, which is coordinated with six oxygen ions, is modeled in two structures. In the structure B-13c the Ce^{4+} cation from the top of the nanoparticle is exchanged. This structure is less stable by 4.8 eV compared to the initial structure B-13a. In the other structure, B-13d, a cation from the bottom layer of the nanoparticle is exchanged and this structure is by 3.9 eV less stable than the initial structure B-13a.

3.2.4. Reduced ceria nanoparticle

One of the structures of reduced $Ce_{13}O_{25}$ nanoparticle, B-13e, is shown in Fig. 5. This structure is obtained by removal of one two-fold coordinated oxygen center from structure B-13a. In the optimized structure both Ce^{3+} cations are located at the bottom layer of the nanoparticle. The energy for the oxygen vacancy formation is 1.2 eV, which is 1.0 eV higher compared to the analogues structure for (100) surface, structure A-13j, but on the other hand is by 1.6 eV lower than the E_{vac} for CeO_2(111) surface. We also considered exchange of a cerium cation from the top of the reduced nanoparticle with Al^{3+} inside the slab, which is

bound to four oxygen atoms (Fig. 5, str. B-13f). In the optimized structure the exchanged cerium ion remains Ce^{4+} and both Ce^{3+} ions are located again in the bottom layer of the nanoparticle. The exchange is unfavorable by 5.2 eV (Table 4). As a consequence the calculated energy for the formation of an oxygen vacancy is very high, 11.2 eV (with respect to B-13a).

3.3. Deposition of single rhodium atom on γ-Al_2O_3(100) surface

Based on the results for the two surfaces, we have chosen γ-Al_2O_3(100) surface to deposit one rhodium atom on different positions in structures with one CeO_2 unit or with the deposited ceria nanoparticle, since the incorporation of ceria species in cavities of the support is favorable only for this surface. Table 5 summarizes the results and figure 6 shows the optimized structures. We modeled three types of structures of deposited rhodium atoms with: i) one CeO_2 unit on the alumina surface; ii) one CeO_2 unit in a cavity of the support; and iii) a $Ce_{13}O_{26}$ nanoparticle on the alumina surface. In all modeled structures one Ce^{4+} cation is reduced to Ce^{3+} and the rhodium atom is oxidized to Rh^+ due to electron transfer from the rhodium atom to the cerium one, as reported earlier for rhodium adsorbed on CeO_2(111) surface.[34-36]

The first structure, A-Rh-1a, is obtained from structure A-1a, where rhodium is deposited far away from the CeO_2 unit (the Rh-Ce distance is 872 pm) and is coordinated to four oxygen centers with an averaged Rh-O distance, <Rh-O>, of 232 pm (Fig. 6, str. A-Rh-1a). The adsorption energy of rhodium is -3.3 eV. In the structure A-Rh-1b the rhodium and cerium ions on the surface are significantly closer, at 415 pm and the structure is more stable by 1.0 eV than A-Rh-1a with adsorption energy of rhodium of -4.4 eV. The Rh^+ ion is bound to two oxygen ions from the surface and one oxygen center from the deposited CeO_2 unit with <Rh-O> value of 214 pm.

Structure A-Rh-1c is the most stable structure of all modeled structures with rhodium and one CeO_2 unit. It is obtained from the structure A-1b with one CeO_2 unit in a subsurface cavity and in it rhodium is coordinated to four oxygen centers, one of which is bound also with the cerium ion. The average <Rh-O> bond length is 235 pm, while the Rh-Ce distance is 381 pm. The number of oxygen neighbors of cerium cation decreases from eight in the structure without rhodium, A-1b, to six, and the <Ce-O> distance increases by 9 pm, likely due to the decrease of the charge of the cerium ion. The structure A-Rh-1c is by 1.4 eV more

stable than the structure A-Rh-1a and the adsorption energy of rhodium is -3.5 eV. This value is very close to the calculated adsorption energy of a rhodium atom on CeO_2(111) surface, -3.7 eV, reported recently.[35]

In structure A-Rh-1d, ceria unit is located in an internal cavity, while rhodium is deposited on the surface, hence Rh-Ce distance is 834 pm. This structure is 2.8 eV less stable than the structure A-Rh-1a. The coordination number of rhodium is 3 and the <Rh-O> value is 231 pm. The adsorption energy of rhodium is by 0.4 eV lower than the corresponding value in structure A-Rh-1a. The energy differences between different structures with rhodium are determined mainly by the relative stability of the corresponding structures without rhodium, as reported in Table 1. The energetic differences with respect to the structure with deposited CeO_2 unit on the surface (structure A-Rh-1a) are almost the same as in the case without rhodium: -1.4 eV (str. A-Rh-1c) and 2.8 eV (str. A-Rh-1d) for systems with rhodium versus -1.3 eV (str. A-1b) and 2.4 eV (str. A-1c) for corresponding systems without rhodium.

In the first structure of deposited rhodium atom in presence of the ceria nanoparticle, A-Rh-13a, rhodium was located initially at the interface of the alumina and $Ce_{13}O_{26}$ nanoparticle, but during the optimization it moved slightly away from the nanoparticle. In the optimized structure the shortest Rh-Ce distance is 432 pm and rhodium is bound only to two oxygen ions from the surface at Rh-O bond lengths of 190 and 205 pm, i.e. by 15 to 30 pm shorter than in structures with one CeO_2 unit. The adsorption energy of rhodium in that structure is -5.2 eV, the highest among the systems, which we modeled. The rhodium species in the second modeled structure with ceria nanoparticle, A-Rh-13b (see Fig. 6), are located closer to Ce^{4+} cation, at Rh-Ce distance of 392 pm. rhodium ion is coordinated to four oxygen centers from alumina surface with <Rh-O> distance of 233 pm and the structure is by 1.3 eV less stable than the first one.

In order to simulate oxidation state of rhodium center under stronger oxidizing conditions we modeled structures with an additional oxygen atom presumably originating from gas-phase oxygen molecule. Recently analogous approach was applied for modeling of platinum ions on ceria nanoparticle.[37] These calculations were performed for RhO species on the models A-1a and A-13a. In both cases the spin density distribution suggested reduction of one Ce^{4+} ion to Ce^{3+}, i.e. the total charge of RhO species is 1+. Thus, the additional oxygen atom causes further oxidation of the rhodium ion.

4. Discussion

4.1. Supported ceria species versus extended ceria surfaces and nanoparticles

Our results showed that the deposition of one or two CeO_2 units or of a ceria nanoparticle is on (001) surface of alumina is less favorable than on (100) surface when they are compared to the corresponding pristine alumina surface and ceria units from CeO_2 (111) slab.[38] Further, the process of incorporation of CeO_2 units is not favorable in the (001) surface in none of the modeled structures, while for in the (100) surface, the incorporation of one and two units in subsurface cavities is favorable with respect to deposited three-dimensional ceria nanoparticle. The exchange of Ce^{4+} cation with aluminum is favorable only on the (100) surface, likely due to the presence of surface three-coordinated aluminum cations, which are less restricted by the framework of the support than the four- and five- coordinated ions. Hence, these results suggest that deposition and/or incorporation of CeO_2 species (taken from a CeO_2(111) slab) on/in alumina surfaces is favorable in the case of the γ-Al_2O_3(100) surface, but not the γ-Al_2O_3(001). These results may be explained with better saturation and lower flexibility of the (001) surface compared to (100) surface of the alumina (see the discussion in the next subsection). Since the (100) surface is more flexible, it accommodates easier ceria species in subsurface cavities. Figure 8 summarizes the main conclusions from the relative stability and reducibility of ceria species on (100) and (001) surfaces of γ-Al_2O_3.

Deposition of the small ceria nanoparticle on both alumina surfaces is exothermic, but it is bound stronger on γ-Al_2O_3(100) surface than on (001) surface, -15.6 eV and -9.8 eV, respectively.

The process of removal of an oxygen atom in the structures with two ceria units on each of the modeled alumina surfaces is strongly endothermic; E_{vac} is between 2.6 and 8.3 eV. Migani et al.[26,31] showed that the formation of single oxygen vacancies in stoichiometric ceria nanoparticles $(CeO_2)_n$ are the lowest when low (two-fold) coordinated oxygen atoms from ceria species are removed and the E_{vac} value varies from 0.46 eV (n=80) to 1.67 eV (n=21). From our models with supported ceria nanoparticle, we removed an oxygen center from the top of the nanoparticle, where oxygen centers are coordinated only with two Ce^{4+} cations. For the models on the γ-Al_2O_3(100) surface the process is very weakly endothermic, 0.2 - 0.3 eV, which implies that the process of oxygen vacancy formation may occur spontaneously under room temperature in such systems. The reduction of ceria particle deposited on (001) surface of alumina is by about 1 eV higher, 1.2 eV, but it is still lower than the E_{vac} value for the regular ceria surfaces, (111), (110) or (100), as well as for some of the ceria nanoparticles.[26,31]

4.2. Distortion of γ-alumina support

We calculated the averaged displacement of aluminum and oxygen ions of the alumina for some of the stoichiometric structures (see Table S1). In general, for both surfaces the average displacement of aluminum and oxygen (all ions respectively surface ions only) of γ-Al_2O_3 increases with the number of incorporated ceria units and is always smaller for the structures with deposited ceria species. The surface atoms move more than the atoms inside the slab. Comparing the average displacements of all aluminum and oxygen ions on Al_2O_3(100) and Al_2O_3(001) surfaces, the displacements are smaller for the structures on the (001) surface by 14.4-32.2 pm compared to the calculated values for the corresponding structures of the (100) surface. Exceptions are the two structures with deposited $Ce_{13}O_{26}$ nanoparticle, where this difference reduces to about 4.0 pm. For structures with deposited or incorporated one and two ceria species there is significant displacement not only of the centers surrounding those species but also of the surface aluminum and oxygen ions (in some case by more than 100 pm). In the case of (001) surface for the structures the average displacement of all surface ions of γ-Al_2O_3 is smaller by 2.0 to 7.0 pm compared to the displacement for the analogues structures of (100) surface.

4.3. Implications for catalysis on CeO_2/γ-Al_2O_3 systems

Our data rationalize the experiments of Duarte et al.[16] , which showed that samples, in which ceria was deposited on alumina contain substantial amounts of Ce^{3+} ions even under oxidizing conditions. Our computational results confirm that incorporation of cerium ions in the subsurface cavity is favorable with respect to CeO_2 unit and to ceria nanoparticle deposited on the γ-Al_2O_3(100) surface. However, our results showed such incorporated cerium ions are stable as Ce^{4+} ions and their reduction to Ce^{3+} ions is more endothermic than that of the cerium ions on the surface of the support. The calculations suggest an explanation of the experimental observation of a large fraction of Ce^{3+} by the strong reduction of the energy for oxygen vacancy formation in ceria nanoparticle supported on the γ-Al_2O_3(100) surface. The calculated E_{vac} values for $Ce_{13}O_{26}$/γ-Al_2O_3(100) system are only 0.2 – 0.3 eV, while on (001) surface the value is higher, 1.2 eV, but still about twice lower than E_{vac} for CeO_2(111) surface.[31,31] This suggests that Ce^{3+} ions can exist as part of small nanoparticles on the alumina (100) surface even after oxidation at room temperature and higher. Complete re-

oxidation of the ceria nanoparticle requires a temperature below room temperature and high oxygen pressure. Such Ce^{3+} ions bind water weaker than Ce^{4+} ions explaining their low reactivity with water at high temperature. Ce^{3+} ions are also formed spontaneously when rhodium atoms are introduced in the system. The presence of rhodium thus stabilizes the presence of reduced cerium ions. This process occurs even when cerium and rhodium are not in direct contact on the alumina surface and contributes to the stability of Ce^{3+} species upon re-oxidation of the samples.

Our theoretical results show that mixed CeO_2/Al_2O_3 and $Rh/CeO_2/Al_2O_3$ systems have significant potential for catalytic applications. For instance, we found that for isolated CeO_2 units the most stable positions on γ-Al_2O_3(100) surface are in the subsurface region. This means that cerium ions are close to the surface and may affect the chemistry on the surface or even do the catalysis themselves. Small ceria particles deposited on Al_2O_3, such as the modeled $Ce_{13}O_{26}$ moieties, show an ability to release part of their oxygen atoms essentially spontaneously (see Fig. 7), hence Ce^{3+} will be present under reaction conditions and can influence the catalytic performance of such systems. The easy release of the oxygen from supported ceria particles due to low oxygen vacancy formation energy may allow to achieve the maximal oxygen storage capacity of ceria, up to 25% of oxygen atoms, i.e., one oxygen atom per two cerium ions as in the transformation from CeO_2 to Ce_2O_3. Three-component $Rh/CeO_2/Al_2O_3$ systems are even more interesting from a catalytic point of view, since Rh spontaneously provides an electron to a Ce^{4+} cation and two species with potential catalytic activity are formed, Rh^+ and Ce^{3+} species. This important knowledge helps to rationalize the available experimental data on the catalytic activity of $Rh/CeO_2/Al_2O_3$ systems in methane steam reforming and can provoke more deep analysis for searching on other interesting catalytic applications of those systems.

5. Summary

Among the modeled structures the incorporation of Ce^{4+} ion in cavities of γ-Al_2O_3 is favored with respect to the ion on the surface only when the ceria species is included in subsurface cavities of the (100) surface. The incorporation of cerium ions in subsurface cavities is exothermic with respect to a ceria nanoparticle $Ce_{13}O_{26}$ deposited on the (100) surface of γ-Al_2O_3. The most favorable is, however, the structure in which one of the CeO_2 units from the top layer of the nanoparticle is moved to alumina surface, which suggest a preference for

formation of a surface layer of ceria on this alumina surface instead of growing as three-dimensional moieties.

The exchange of Ce^{4+} by Al^{3+} in the model with deposited ceria nanoparticle is essentially energy neutral for the structures with exchanged Ce^{4+} from the top of the ceria nanoparticle, while it is significantly endothermic for the structures with exchanged Ce^{4+} from the bottom of the nanoparticle (at the interface with the alumina surface). The attempts to model incorporation of Ce^{3+} within internal cavities of the γ-Al_2O_3 slab using the $Ce_{13}O_{26}/Al_2O_3(100)$ or $Ce_{13}O_{26}/Al_2O_3(001)$ model system were not successful – the Ce^{3+} ions were created on the ceria nanoparticle which is adsorbed on the surface, while incorporated ceria species remain oxidized as Ce^{4+}.

The deposition of small ceria nanoparticle, $Ce_{13}O_{26}$, on (100) and (001) surfaces of γ-Al_2O_3 strongly reduces the energy for oxygen vacancy formation to an essentially spontaneous process on (100) surface, which may be a reason for the experimentally detected Ce^{3+} ions in CeO_2/γ-Al_2O_3 systems even after re-oxidation.[16]

In all modeled structures with deposited rhodium atom or RhO moiety on alumina-supported ceria the calculations show electron transfer from rhodium to a cerium ion resulting in reduction of Ce^{4+} to Ce^{3+} and the oxidation of the rhodium center. Only in presence of such deposited rhodium atoms the cerium ions incorporated inside alumina are reduced to Ce^{3+}.

Acknowledgments

Support by the FP7 program of the European Union (project Beyond Everest and COST Action CM1104), and CPU time on BG/P at Bulgarian Supercomputing Center is gratefully acknowledged.

Electronic supplementary information: Figures with all optimized structures on (100) and (001) γ-Al_2O_3 slabs. Table with average displacement of Al and O ions of (100) and (001) γ-Al_2O_3 slabs. Description of the approach for simulation of the relative concentrations of reduced and stoichiometric ceria nanoparticles.

References

1. A. Trovarelli, *Catalysis by Ceria and Related Materials.* Imperial College Press, UK, 2002.

2. Y-L. Song, L-L. Yin, J. Zhang, P. Hu, X-Q. Gong and G. A. Lu, *Surf. Sci.*, 2013, **618**, 140-147.

3. G. Kim, *Ind. Eng. Chem. Res.,* 1982, **21**, 267-274.

4. J. Paier, C. Penschke and J. Sauer, *Chem. Rev.,* 2013, **113**, 3949–3985.

5. B.C.H. Steele, A. Heinzel, *Nature,* 2001, **404**, 345-352.

6. E. C. Su and W.G. Rothschield, *J.Catal.,* 1986, **99**, 506-510.

7. T. Q. Nguyen, M. C. S. Escaño, H. Nakanishi, H. Kasai, H. Maekawa, K. Osumi and K. Sato, *Appl. Surf. Sci.,* 2014, **288**, 244-250.

8. M. Cargnello, V. V. T. Doan-Nguyen, G. R. Gordon, R. E. Diaz, E. A. Stach, R. J. Gorte, P. Fornasiero and C. B. Murray, *Science,* 2013, **341**, 771-773.

9. K. Sohlberg, S. Pennycook and S. T. Pantelides, *J. Am. Chem. Soc.,* 1999**, 121**, 10999-11001.

10 C. Y. Ouyang, Ž. Šljivančanin and A. Baldereschi, *Phys. Rev. B.,* 2009, **79**, 235410-235417.

11. H. Knözinger and P. Ratnasamy, *Rev.- Sci. Eng.*, 1978, **17**, 31-70.

12. M. Trueba and St.Trasatti, *Eur. J. Inorg. Chem.*, 2005, **17**, 3393-3403.

13. S. Y. Hosseini and M. R. K. Nikou, *J. Ind. Eng. Chem.*, 2014, **20**, 4421-4428.

14. C. H. Hu, C. Chizallet, C. Mager-Maury, M. Corral-Valero, P. Sautet, H. Toulhoat and P. Raybaud, *J. Catal.*, 2010*,* **274**, 99–110.

15. X. Ge, S. Hu, Q. Sun and J. Shen, *J. Nat. Gas Chem.*, 2003, **12**, 119-122.

16. R. B. Duarte, O. V. Safonova, F. Krumeich, M. Makosh and J. A. van Bokhoven, *ACS Catal.*, 2013, **3**, 1956-1964.

17. I. Cuauhtémoc, G. D. Ángel, G. Torres, C. Angeles-Chavez and E. Ramos, *Top. Catal.*, 2011, **54**, 153-159.

18. X.-R. Shi and D. S. Sholl, *J. Phys. Chem. C* 2012, **116**, 10623-10631.

19. M. Digne, P. Sautet, P. Raybaud, P. Euzen and H. Toulhoat, *J. Catal.*, 2004, **226**, 54-68.

20. J.P. Perdew, J.A. Chevary, S.H. Vosko, K.A. Jackson, M.R. Pederson, D.J. Singh and C. Fiolhais, *Phys. Rev. B*., 1992, **46**, 6671-6687.

21. J.P. Perdew, J.A. Chevary, S.H. Vosko, K.A. Jackson, M.R. Pederson, D.J. Singh and C. Fiolhais, *Phys. Rev. B*., 1993, **48**, 4978-4978.

22. G. Kresse and J. Hafner, *Phys. Rev. B,* 1993, **47**, 558-561.

23. G. Kresse and J. Hafner, *Phys. Rev. B*, 1994, **49**, 14251-14269.

24. G. Kresse and J. Furthmüller, *Comput. Mat. Sci.*, 1996, **6**, 15-50.

25. G. Kresse and J. Furthmüller, *Phys. Rev. B*, 1996, **54**, 11169-11186.

26. A. Migani, G. N. Vayssilov, S. T. Bromley, F. Illas and K. M. Neyman, J. Mater. Chem., 2010, **20**, 10535-10546.

27. G. N. Vayssilov, M. Mihaylov, P. St. Petkov, K. I. Hadjiivanov and K. M. Neyman, *J. Phys. Chem. C*, 2011, **115**, 23435-23454.

28. G. Kresse and D. Joubert, , *Phys. Rev. B*., 1999, **59**, 1758-1775.

29. H. J. Monkhorst and J. D. Pack, *Phys. Rev. B*, 1976, **13**, 5188- 5192.

30. M. Nolan, J. E. Fearon and G. W. Watson, 2006, **177**, 3069-3074.

31. A. Migani, G. N. Vayssilov, S. T. Bromley, F. Illas and K. M. Neyman, *Chem. Commun.*, 2010, **46**, 5936-5938.

32. G. N. Vayssilov, Y. Lykhach, A. Migani, T. Staudt, G. P. Petrova, N. Tsud, T. Skála, A. Bruix, F. Illas, K. C. Prince, V. Matolín, K. M. Neyman and J. Libuda, *Nature Mater.*, 2011, **10**, 310-315.

33. M. Alam, S. M. Kozlov, K. H. Lim, A. Migani, and K. M. Neyman, *J. Mater. Chem. A*, 2014, **2**, 18329-18338.

34. Z. Lu and Z. Yang, *J. Phys.: Condens. Matter.*, 2010, **22**, 475003-475013.

35. K. Hermansson and C.W. M. Castleton, *J. Mater. Chem. A*, 2014, **2**, 2333-2345.

36. Y. M. Choi, M. Scott, T. Söhnel and H. Idriss, *Phys. Chem. Chem. Phys.*, 2014, **16**, 22588-22599.

37. H. A. Aleksandrov, K. M. Neyman, and G. N. Vayssilov *Phys. Chem. Chem. Phys.*, 2015, **17**, 14551-14560.

38. M. Y. Mihaylov, E. Z. Ivanova, H. A. Aleksandrov, P. St. Petkov, G. N.Vayssilov, K. I. Hadjiivanov, *Chem. Commun.*, 2015, **51**, 5668-5671.

Tables

Table 1. Energetic and structural parameters for one or two CeO_2 units on γ-Al_2O_3(100) surface: relative energies for incorporation of CeO_2 unit(s) or exchange of cerium ion with Al^{3+} ion (ΔE, eV); oxygen vacancy formation energy (E_{vac}, eV), number of all oxygen neighbors of cerium cations (N); average distance between cerium and oxygen ions <Ce-O>, and distance between cerium cations r(Ce-Ce) in pm.

Structure	Description	ΔE	E_{vac}	N	<Ce-O>	r(Ce-Ce)
	one CeO_2 unit					
A-1a	CeO_2 deposited	0.0		3	204	
A-1b	CeO_2 in subsurface cavity	-1.3		8	243	
A-1c	CeO_2 in internal cavity	2.4		7	243	
A-1d	exchange Ce^{4+} with surface Al^{3+}(3O)	-0.7		5	226	
A-1e	exchange of Ce^{4+} with surface Al^{3+}(5O)	-0.1		5	226	
A-1f	exchange of Ce^{4+} above surface Al^{3+}(5O)	0.2		6	237	
A-1g	exchange of Ce^{4+} with internal Al^{3+}(4O)	1.1		7	242	
A-1h	exchange of Ce^{4+} with internal Al^{3+}(4O)	2.8		7	238	
A-1i	exchange of Ce^{4+} with internal Al^{3+}(6O)	4.7		6	220	
	two CeO_2 units					
A-2a	$2CeO_2$ deposited	0.0		4[a], 4[a]	219[a], 214[a]	395
A-2b	$1CeO_2$ deposited, $1CeO_2$ in subsurface cavity	1.6		4[a], 8[b]	216[a], 243[b]	445
A-2c	$2CeO_2$ in identical subsurface cavities	2.3		7[b], 7[b]	238[b], 239[b]	810
A-2d	$1CeO_2$ subsurface, $1CeO_2$ internal cavity	2.9		8[b], 7[b]	241[b], 245[b]	1039
A-2e	$2CeO_2$ internal cavities	4.5		7[b], 7[b]	237[b], 242[b]	642
	one Ce_2O_3 unit (obtained from structure with two CeO_2 units)					
A-2f	Ce_2O_3 deposited	0.0	3.1	3[a], 4[a]	222[a], 229[a]	360
A-2g	Ce_2O_3 in subsurface cavity	0.5	3.6	7[b], 7[b]	245[b], 250[b]	408
A-2h	$1Ce^{3+}$ in subsurface, 1 Ce^{3+} in internal cavity	5.8	8.9	5[b], 7[b]	250[b], 246[b]	474
A-2i	exchange of $2Ce^{3+}$ with internal $2Al^{3+}$	5.2	8.3	7[b], 7[b]	247[b], 249[b]	789

[a] deposited cerium cations
[b] incorporated or exchanged cerium cations

Table 2. Energetic and structural parameters for stoichiometric or reduced $Ce_{13}O_{26}$ nanoparticle on γ-Al_2O_3(100) surface: relative energies for incorporation of CeO_2 unit(s) or exchange of cerium ion with Al^{3+} ion (ΔE, eV); oxygen vacancy formation energy (E_{vac}, eV), number of all oxygen neighbors of cerium cations (N); average distance between cerium and oxygen ions <Ce-O>, and distance between cerium cations r(Ce-Ce) in pm.

Structure	Description	ΔE	E_{vac}	N	<Ce-O>	r(Ce-Ce)
	stoichiometric nanoparticle					
A-13a	$Ce_{13}O_{26}$ deposited	0.0				
A-13a'	$Ce_{12}O_{24}$ deposited, $1CeO_2$ deposited	-0.9		5	222	
A-13a"	$Ce_{12}O_{24}$ deposited, $1CeO_2$ deposited	-1.8		5	230	
A-13b	$Ce_{12}O_{24}$ deposited, $1CeO_2$ subsurface	-1.4		7	238	
A-13c	$Ce_{11}O_{22}$ deposited, $2CeO_2$ subsurface	-0.6		7[a], 7[a]	234[a], 234[a]	414
A-13d	$Ce_{13}O_{26}$, exchange of top $1Ce^{4+}$ with Al^{3+}	0.0		7	238	
A-13e	$Ce_{13}O_{26}$, exchange of top $1Ce^{4+}$ with Al^{3+}	0.1		7	233	
A-13f	$Ce_{13}O_{26}$, exchange of top $1Ce^{4+}$ with Al^{3+}	0.3		7	237	
A-13g	$Ce_{13}O_{26}$, exchange of top $1Ce^{4+}$ with Al^{3+}	0.4		7	237	
A-13h	$Ce_{13}O_{26}$, exchange of bottom $1Ce^{4+}$ with Al^{3+}	1.5		7	238	
A-13i	$Ce_{13}O_{26}$, exchange of bottom $1Ce^{4+}$ with Al^{3+}	1.9		7	238	
	reduced nanoparticle					
A-13j	$Ce_{13}O_{25}$ deposited	0.0	0.2			
A-13k	$Ce_{13}O_{25}$ deposited	0.1	0.3			
A-13l	$Ce_{12}O_{23}$ deposited, $1CeO_2$ subsurface	0.0	0.2	7	237	
A-13m	$Ce_{12}O_{23}$ deposited, $1Ce^{3+}$ and $1CeO_2$ in subs.	1.0	1.1	6[b], 7[a]	241[b], 234[a]	477
A-13n	$Ce_{13}O_{25}$, exchange of $1Ce^{4+}$ with Al^{3+} internal	2.8	3.0	7	236	

[a] incorporated or exchanged Ce^{4+} cations

[b] incorporated Ce^{3+} cation

Table 3. Energetic and structural parameters for one or two CeO_2 units on γ-Al_2O_3(001) surface: relative energies for incorporation of CeO_2 unit(s) or exchange of cerium ion with Al^{3+} ion (ΔE, eV); oxygen vacancy formation energy (E_{vac}, eV), number of all oxygen neighbors of cerium cations (N); average distance between cerium and oxygen ions <Ce-O>, and distance between cerium cations r(Ce-Ce) in pm.

Structure	Description	ΔE	E_{vac}	N	<Ce-O>	r(Ce-Ce)
	one CeO_2 unit					
B-1a	CeO_2 deposited	0.0		5	235	
B-1b	CeO_2 subsurface cavity	3.8		6	235	
B-1c	CeO_2 internal cavity	11.3		8	236	
B-1d	exchange of Ce^{4+} with surface Al^{3+}(5O)	1.7		5	223	
B-1e	exchange of Ce^{4+} with internal Al^{3+}(4O)	3.0		8	246	
	two CeO_2 units					
B-2a	$2CeO_2$ deposited	0.0		5[a], 5[a]	237[a], 234[a]	650
B-2b	$2CeO_2$ in identical subsurface	8.1		8[b], 8[b]	241[b], 241[b]	550
	four CeO_2 units					
B-4a	$4CeO_2$ deposited	0.0				
B-4b	$3CeO_2$ deposited, $1CeO_2$ subsurface	0.7		7[b]	227[b]	
	one Ce_2O_3 unit (obtained from structures with two CeO_2 units)					
B-2c	Ce_2O_3 deposited	0.0	2.6	4[a], 4[a]	240[a], 239[a]	675
B-2d	two Ce^{3+} in identical subsurface	1.1	3.7	6[b], 6[b]	251[b], 249[b]	400

[a] deposited cerium cations

[b] incorporated or exchanged cerium cations

Table 4. Energetic and structural parameters for stoichiometric or reduced $Ce_{13}O_{26}$ nanoparticle on γ-Al_2O_3(001) surface: relative energies for incorporation of CeO_2 unit(s) or exchange of cerium ion with Al^{3+} ion (ΔE, eV); oxygen vacancy formation energy (E_{vac}, eV), number of all oxygen neighbors of cerium cations (N); average distance between cerium and oxygen ions <Ce-O> in pm.

Structure	Description	ΔE	E_{vac}	N	<Ce-O>
	stoichiometric nanoparticle				
B-13a	$Ce_{13}O_{26}$ deposited	0.0			
B-13b	$Ce_{12}O_{24}$ deposited, $1CeO_2$ subsurface	8.7		6[a]	237[a]
B-13c	$Ce_{13}O_{26}$, exchange of top $1Ce^{4+}$ with internal Al^{3+}	4.8		7[a]	232[a]
B-13d	$Ce_{13}O_{26}$, exchange of bottom $1Ce^{4+}$ with internal Al^{3+}	3.9		7[a]	231[a]
	reduced nanoparticle				
B-13e	$Ce_{13}O_{25}$ deposited	0.0	1.2		
B-13f	$Ce_{13}O_{25}$, exchange of $1Ce^{4+}$ with internal Al^{3+}	5.2	11.2	6[a]	237[a]

[a] incorporated or exchanged cerium cations

Table 5. Energetic and structural parameters of the structures with deposited rhodium atom. Relative stability (ΔE, eV) and adsorption energy of rhodium atom (E_{ads}, eV); the number of oxygen neighbors of Rh (M); number of the oxygen neighbors of Ce (N); average distance between cerium and oxygen cations <Ce-O>, and distance between rhodium and cerium cations r(Rh-Ce^{3+}) in pm.

Structure	Description	ΔE	E_{ads}	r(Rh-Ce^{3+})	M	<Rh-O>	N	<Ce-O>
A-Rh-1a	Rh deposited, CeO_2 deposited	0.0	-3.3	872	4	232	3	207
A-Rh-1b	Rh deposited, CeO_2 deposited	-1.0	-4.4	415	3	214	4	228
A-Rh-1c	Rh deposited, CeO_2 subsurface	-1.4	-3.5	381	4	235	6	252
A-Rh-1d	Rh deposited, CeO_2 internal	2.8	-2.9	834	3	231	6	245
A-Rh-13a	Rh deposited, $Ce_{13}O_{26}$ deposited	0.0	-5.2	668	2	198		
A-Rh-13b	Rh deposited, $Ce_{13}O_{26}$ deposited	1.3	-3.9	989	4	233		
A-RhO-1a	RhO deposited, CeO_2 deposited		-1.8[a]	855	4	205	3	217
A-RhO-13a	RhO deposited, $Ce_{13}O_{26}$ deposited		-0.8[a]	685	3	196		

[a] energy gain from the adsorption of ½ O_2 to the corresponding structure without the additional oxygen.

Figures

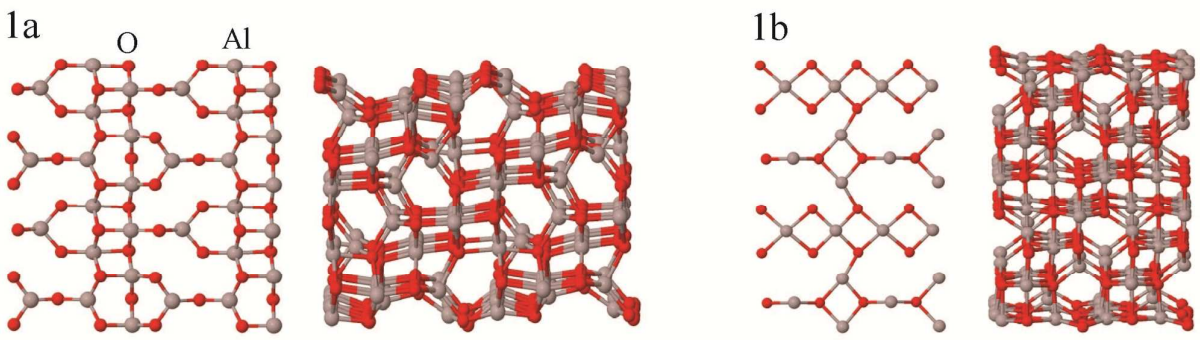

Figure 1. Top and side view of the studied surfaces: a) γ-Al_2O_3(100); b) γ-Al_2O_3(001). The gray and red spheres represent Al and O, respectively.

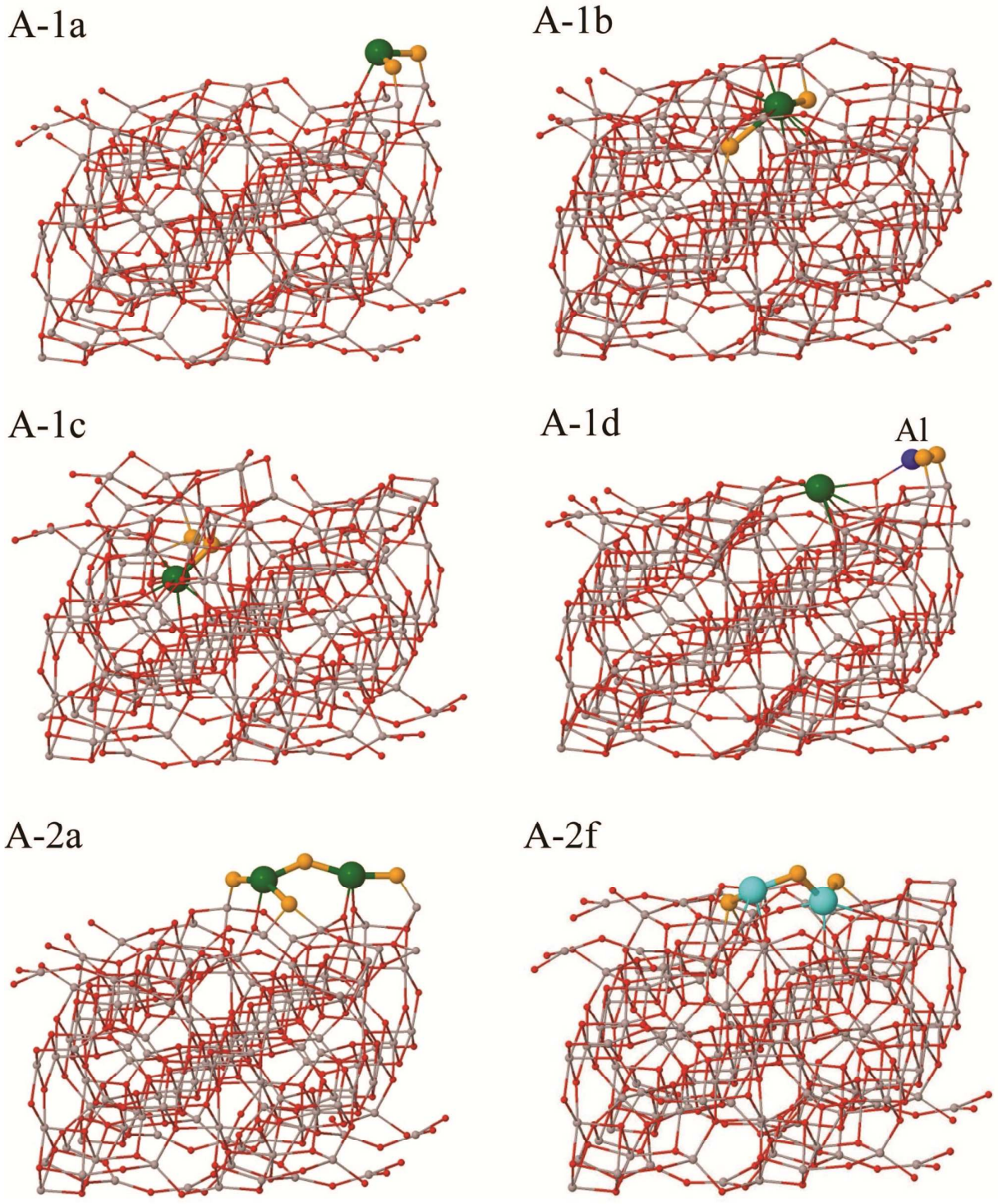

Figure 2. Selected optimized structures of stoichiometric or reduced ceria units on γ-Al_2O_3(100): A-1a-one deposited unit; A-1b-one unit CeO_2 in a subsurface cavity; A-1c- one unit CeO_2 in an internal cavity; A-1d - exchanged Ce^{4+} cation from the deposited CeO_2 unit with three coordinated surface Al^{3+} cation; A-2a - two deposited ceria units; A-2f -deposited Ce_2O_3 unit. Ce^{4+}-green, Ce^{3+}-cyan, O from CeO_2 species-orange, Al-gray, O-red, exchanged Al-dark blue.

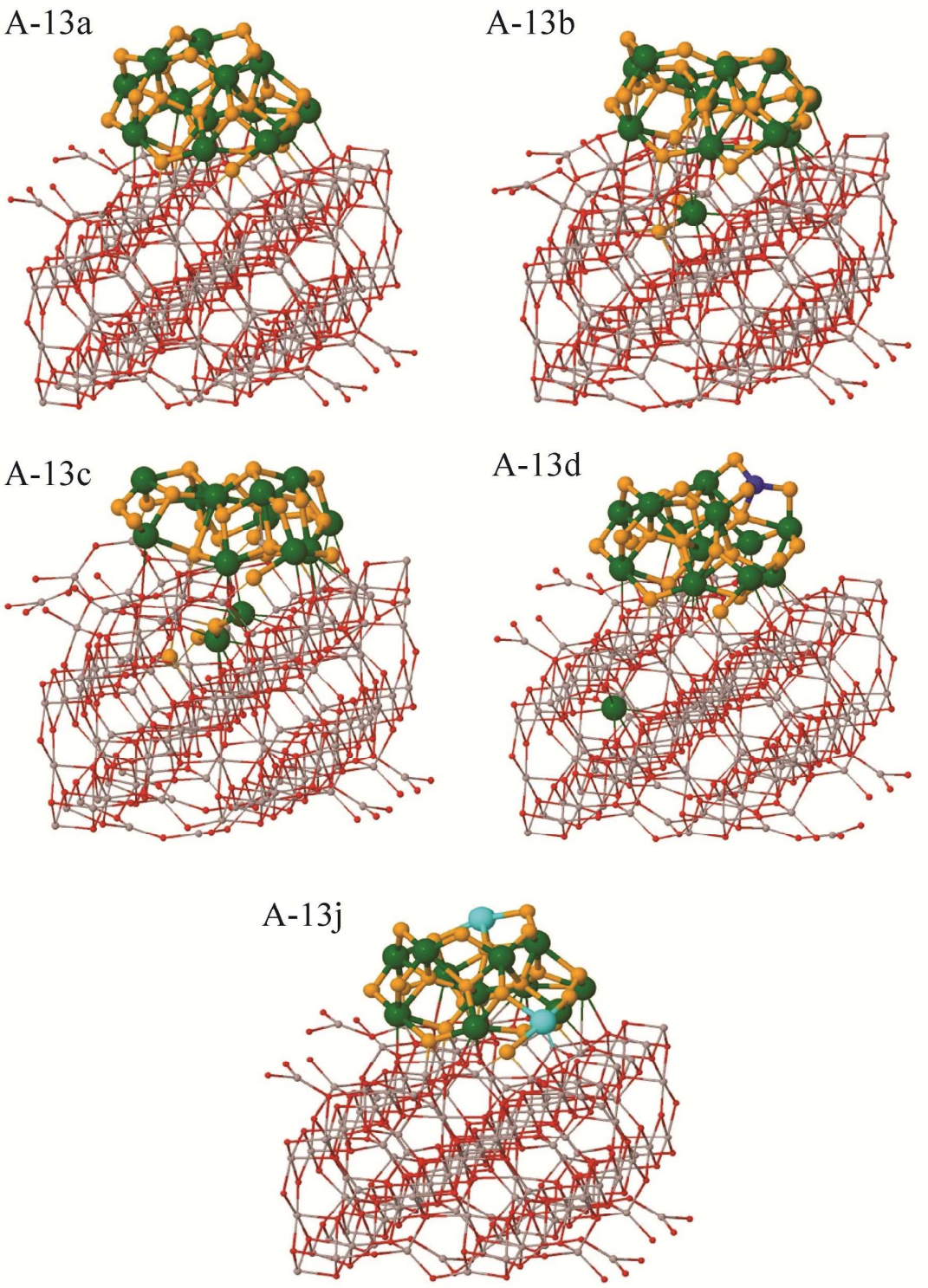

Figure 3. Selected optimized structures of stoichiometric or reduced ceria nanoparticle on γ-Al_2O_3(100): A-13a-deposited $Ce_{13}O_{26}$ nanoparticle; A-13b - deposited $Ce_{12}O_{24}$ nanoparticle and one CeO_2 unit in subsurface cavity, A-13c- deposited $Ce_{11}O_{22}$ nanoparticle and two CeO_2 units in subsurface cavities; A-13d - one of the top Ce^{4+} cations is exchanged with Al^{3+} from the bulk; A-13j - deposited reduced $Ce_{13}O_{25}$ nanoparticle. Ce^{4+}-green, Ce^{3+}-cyan, O from CeO_2 species-orange, Al-gray, O-red, exchanged Al-dark blue.

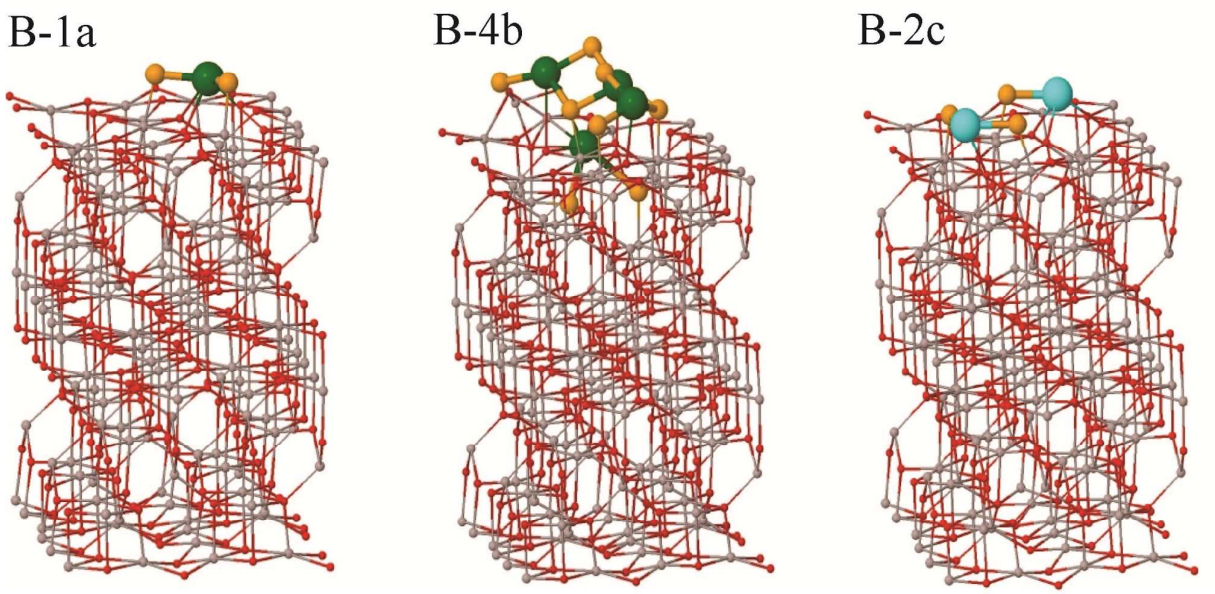

Figure 4. . Selected optimized structures of stoichiometric or reduced CeO_2 species on γ-Al_2O_3(001): B-1a – deposited unit CeO_2, B-4b - 3 deposited CeO_2 units and one in a subsurface cavity; B-2c - two deposited Ce^{3+} cations.

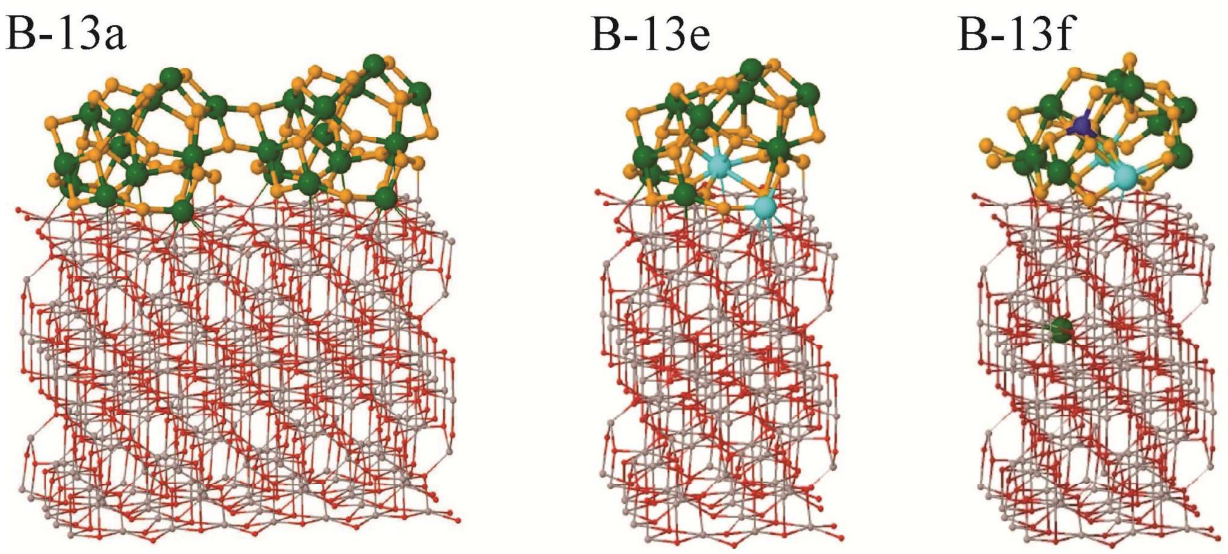

Figure 5. Selected optimized structures of stoichiometric or reduced ceria nanoparticle on γ-Al_2O_3(001): B-13a - deposited $Ce_{13}O_{26}$ nanoparticle; B-13e - deposited $Ce_{13}O_{25}$ nanoparticle and B-13f - exchange of bulk Al^{3+} with Ce^{4+} cation from the top layer of the reduced nanoparticle.

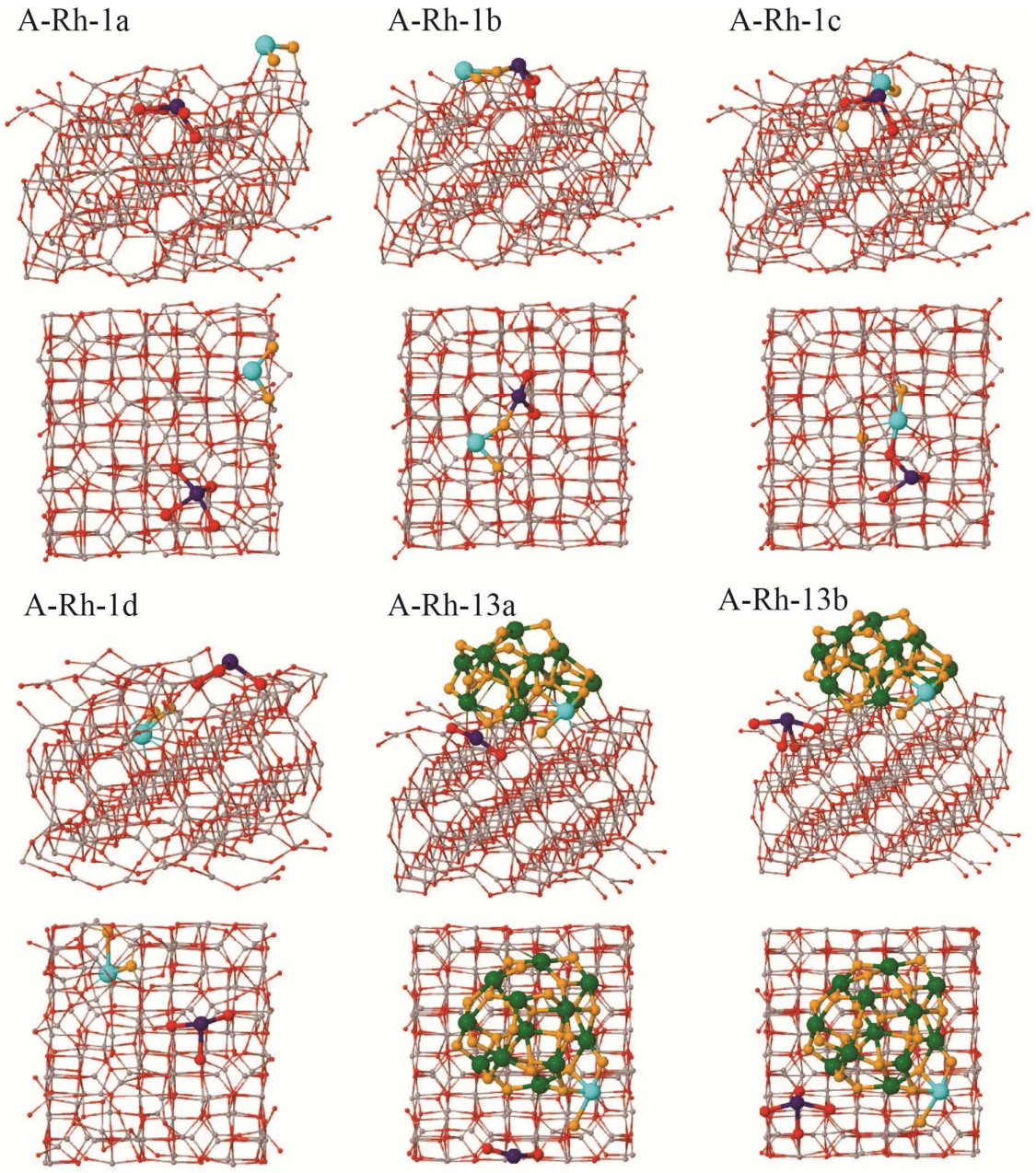

Figure 6. Optimized models of different structures with deposited Rh atom and ceria species on γ-Al_2O_3(100): A-Rh-1a and A-Rh-1b - deposited Rh ion and deposited one CeO_2 unit; A-Rh-1c - deposited Rh and one ceria unit in a subsurface cavity; A-Rh-1d-deposited Rh and one CeO_2 in an internal cavity; A-Rh-13a and A-Rh-13b - deposited Rh and $Ce_{13}O_{26}$ nanoparticle. Rh ion is in indigo, Ce^{3+} – cyan and Ce^{4+} – green.

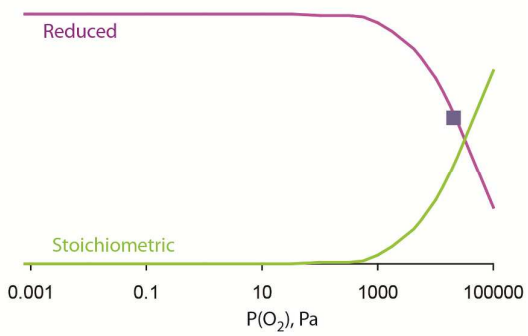

Figure 7. Simulated relative concentration at 300 K of reduced (with one O vacancy) and stoichiometric ceria nanoparticles on γ-Al_2O_3(100) surface using enthalpy and entropy values obtained from computational results. The blue square shows the concentration of reduced species under air at atmospheric pressure.

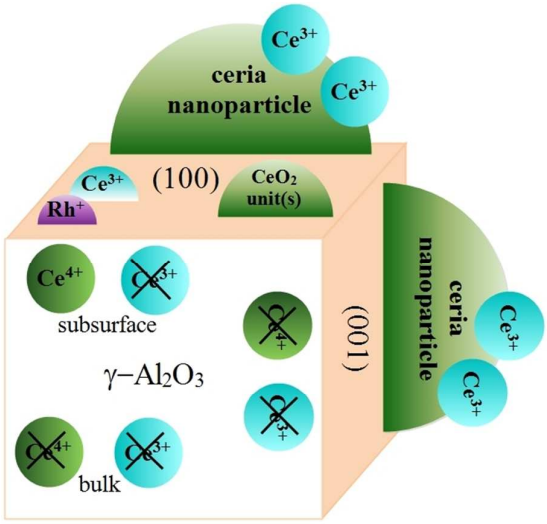

Figure 8. Schematic presentation of the conclusions from the relative stability and reducibility of ceria species on (100) and (001) surfaces of γ-Al_2O_3.

TOC

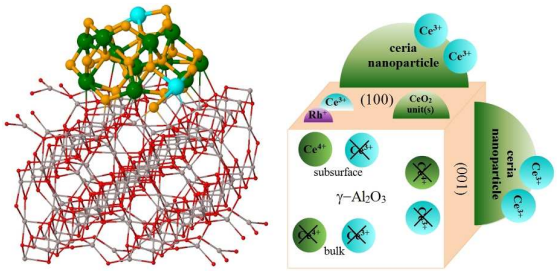

Computational modeling suggests that ceria nanoparticle deposited on γ-Al_2O_3 is reduced easier than isolated nanoparticle and incorporation of cerium ions in support cavities is favored on γ-Al_2O_3 (100) surface.